An Analytical Model for Desorption Area in Coal-bed Methane Production Wells

Bingxiang Xu[a,*], Xiangfang Li[a], Manouchehr Haghighi[b] ,Xiyao Du[a], Xinzhou Yang[a], Dong Chen[c], Yuyang Zhai[c]

a. College of Petroleum Engineering，China University of Petroleum, Beijing 102249, China
b. Australian School of Petroleum, The University of Adelaide, SA5005, Australia
c. China United Coalbed Methane Engineering Research Center Co, Ltd, Beijing 100095, China
*Corresponding author: College of Petroleum Engineering，China University of Petroleum, Beijing 102249, China.
Tel.: +86 1089734340; Fax: +86 1089734951; Email: xubingxiang8526@163.com

Abstract:

Production forecasting, well spacing, and well pattern optimization are key tasks in coal-bed methane field development plan. Desorption area around a production well is an important factor in well performance and reserve estimation. Analytical models are found to be simple and practical tools for drainage area calculation and well deliverability in conventional reservoirs. However, up to now, we have found no such analytical model for coal-bed methane wells with two-phase flow in which the gas desorption in coal is the controlling mechanism while the water is flowing in the cleat system.

In this paper, we present a mathematical model to predict how the size of desorption area is changing with pressure propagation during gas and water production. The pressure profiles at different production stages are determined using diffusivity equation which is solved using the known method of “continuous succession of steady states”. For the case of two-phase flow of gas-water system, the pressure squared concept is used for linearization in middle and late times, while the pressure concept is used in early times when water flow is dominated. We have combined pressure from the solution of diffusivity equation with the material balance equation in order to develop our predictive model which is applicable for vertical wells for both cases of with or without hydraulic fractures.

This model is verified by numerical simulation and is in excellent agreement with the numerical solutions. Furthermore, the developed model is applied in one coal-bed methane well group in Hancheng field in China. It is found that desorption area is expanded outward in elliptical shape and the area can be calculated by the gas production data. The results show that two sample wells in the group have interfered with each other after producing for 525 days.

Key words: coal-bed methane; desorption area; gas-water two-phase flow; hydraulic fracture; predictive models

1. Introduction

In coal-bed methane reservoirs, the gas is mainly stored in micro pores of coal surface by the mechanism of adsorption in contrary with the conventional reservoirs which free gas is stored in rock porosity system [1-4]. To release the adsorbed gas from the coal surface and to produce it

through the natural cleat system, the reservoir pressure should be reduced to a critical desorption pressure by dewatering operation. During this reservoir depressurizing, the desorption area expands outward with pressure propagation. To date, both analytical [5, 6] and numerical approaches [7, 8] have been used to predict the expansion of desorption area. However, it is found that the previous analytical models are not working accurately in the case of two-phase flow of gas-water system because not only the flow behavior in this case is more complex [3, 9]; but also, the working condition of CBM well is frequently changing as a result of work-over, shut-in well, and so on. In the case of numerical modeling, many different data set are required to run the simulation such as the geological model, coal and fluid properties [8, 10] and petrophysical properties for example permeability, porosity, and relative permeability curves which are hard to obtain [11]. In contrary to numerical simulation, an analytical model does not need most of those data sets and it is simple and fast.

In this paper, we first present different mechanisms of pressure propagation and desorption area expansion during the production. Then, a simplified mathematical model is developed for the pressure distribution in CBM based on the characteristic of gas-water ratio. Furthermore, the pressure equations are solved using the method of continuous succession of steady states. Next, a mathematical model for desorption area in a coal-bed methane well is developed combined with material balance equation. Then, it is shown that the developed new model is validated with numerical simulation. Finally, the predictive model has been applied in Hancheng CBM field in China and the results are discussed in detail. Some conclusions are presented in the last section.

2. Pressure propagation and desorption area expansion

It is necessary to review different flow mechanisms occurring in CBM reservoirs for the development of a mathematical modeling. Throughout the production from under-saturated CBM reservoirs, the following three stages are commonly taking place: 1- dewatering stage; 2- stable production stage; and 3- decline stage [3]. In all three stages, either single-phase or two-phase flows can occur depending on the relative permeability of each phase. During the early stage of depressurizing, since no gas has been desorbed, single phase water flows only. Once the pressure reaches the critical desorption pressure, the gas phase will change from adsorbed gas to free gas state. By the time the gas phase reaches the critical gas saturation, a two-phase gas-water flow will develop in the cleat system. As a result, the following characteristics for pressure propagation in each stage will occur:

(1) During the dewatering stage, since the flow behavior is only a single phase, the pressure propagates through the water in the cleat system. The pressure propagation will interfere with other neighboring wells at the flow boundary. After reaching to the boundary, the pressure drop in the drainage area will be proportional to the water production rate.

(2) During stable stage, since the reservoir pressure is reduced to the critical desorption pressure, and the gas begins to desorb and diffuse through the coal matrix to the cleat system, the

desorption area begins to expand (Figure1). At this time, a single-phase water flow is changed to two-phase flow. In this case, the resulting flow resistance in two-phase system is obviously higher than single phase flow. However, on the other hand, the matrix system acts as a source supplying gas to the cleats therefore, it slows down the trend of pressure drop. In overall, the expansion of desorption area is controlled by both desorption and two-phase flow. The expansion of desorption area will end when desorption front reaches the boundary.

(3) During decline stage, once the gas saturation is at the highest and the water saturation decreases to immobile residual saturation, the flow system becomes a single-phase again; however, this time is gas-flow only.

3. Mathematical Model

3.1 Simplified approach for two-phase flow equation of CBM

The partial differential equations for two-phase flow in coal seam are given in the following equations [12-14]:

$$\text{Gas: } \nabla\left(\frac{KK_{\mathrm{rg}}}{B_{\mathrm{g}}\mu_{\mathrm{g}}}\nabla P\right)=\frac{\partial}{3.6\partial t}\left(\frac{S_{\mathrm{g}}\phi}{B_{\mathrm{g}}}\right)+\frac{q_{\mathrm{d}}}{B_{\mathrm{g}}} \tag{1}$$

$$\text{Water: } \nabla\left(\frac{KK_{\mathrm{rw}}}{B_{\mathrm{w}}\mu_{\mathrm{w}}}\nabla P\right)=\frac{\partial}{3.6\partial t}\left(\frac{S_{\mathrm{w}}\phi}{B_{\mathrm{w}}}\right) \tag{2}$$

The above equations are basically the combination of mass balance and Darcy' law in which the quantity of desorption gas is given by equilibrium sorption model [5]:

$$q_{\mathrm{d}}=C_{\mathrm{d}}\phi\frac{\partial P}{\partial t} \tag{3}$$

Where C_{d} is the desorption compressibility:

$$C_d=\frac{P_{sc}ZTV_m b}{PZ_{sc}T_{sc}\phi\left(1+bP\right)^2} \tag{4}$$

Multiplying Eq. $\nabla\left(\frac{KK_{\mathrm{rg}}}{B_{\mathrm{g}}\mu_{\mathrm{g}}}\nabla P\right)=\frac{\partial}{3.6\partial t}\left(\frac{S_{\mathrm{g}}\phi}{B_{\mathrm{g}}}\right)+\frac{q_{\mathrm{d}}}{B_{\mathrm{g}}}$ (1) by B_{g}, and Eq. $\nabla\left(\frac{KK_{\mathrm{rw}}}{B_{\mathrm{w}}\mu_{\mathrm{w}}}\nabla P\right)=\frac{\partial}{3.6\partial t}\left(\frac{S_{\mathrm{w}}\phi}{B_{\mathrm{w}}}\right)$ by B_{w}, and adding the two equations together, we have:

$$B_g\nabla\left(\frac{K_g}{B_g\mu_g}\nabla P\right)+B_w\nabla\left(\frac{K_w}{B_w\mu_w}\nabla P\right)=\frac{C_t^*\phi\partial P}{3.6\partial t} \tag{5}$$

Where C_t^* is the modified form of total system compressibility and it is given as the following [5]:

$$C_t^*=C_d+C_f+C_gS_g+C_wS_w \tag{6}$$

By expanding the differential operators of the left terms in Eq. (5), we have:

$$\left(\frac{K_g}{\mu_g}+\frac{K_w}{\mu_w}\right)\nabla^2 P + B_w\nabla\left(\frac{K_w}{B_w\mu_w}\nabla P\right)+B_g\nabla\left(\frac{K_g}{B_g\mu_g}\right)\nabla P=\frac{C_t^*\phi\partial P}{3.6\partial t} \qquad (7)$$

The total mobility of gas and water, and gas-water ratio (GWR) are defined in the following two equations:

$$\lambda_t=\frac{K_g}{\mu_g}+\frac{K_w}{\mu_w} \qquad (8)$$

$$GWR=\frac{K_g}{\mu_g B_g}\frac{\mu_w B_w}{K_w} \qquad (9)$$

The third term in Eq. (7) can be written in terms of GWR as:

$$B_g\nabla\left(\frac{K_g}{B_g\mu_g}\right)\nabla P = B_g GWR\nabla\left(\frac{K_w}{\mu_w B_w}\right)\nabla P + B_g\frac{K_g}{\mu_g B_g}\nabla GWR\nabla P \qquad (10)$$

We can simplify the Eq. (7) by defining the early stage of low GWR and later stage of high GWR as following:

(1) Early two-phase flow stage including single-phase water flow (low *GWR*)

In this stage, the gas saturation is around the critical saturation and the gas flow rate is very low, therefore, both GWR and $\nabla GWR\nabla P$ are assumed to be negligible [13]. Thus, Eq. (7) is changed into Eq (11) as following:

$$\nabla^2 P+\nabla\ln\left(\frac{K_w}{\mu_w B_w}\right)\nabla P=\frac{1}{3.6}\frac{C_t^*\phi}{\lambda_t}\frac{\partial P}{\partial t} \qquad (11)$$

It is assumed that the water permeability K_w, water viscosity μ_w and formation volume factor of water B_w are all constant in early production stage, so

$$\frac{K_w}{\mu_w B_w}=\text{const} \qquad (12)$$

Therefore the second term in Eq. (11) becomes zero and the diffusivity equation is:

$$\nabla^2 P=\frac{1}{3.6}\frac{C_t^*\phi}{\lambda_t}\frac{\partial P}{\partial t} \qquad (13)$$

(2) Middle two-phase and late single-phase gas flow stages (High *GWR*)

In these two stages, the gas phase production is dominated while the water rate is declining. In this case, the resulting GWR is high, and 1/GWR can be neglected [12-14]. We can write the second term of Eq. (7) in terms of GWR as the following:

$$B_w\nabla\left(\frac{K_w}{B_w\mu_w}\right)\nabla P = B_w\left(\frac{1}{GWR}\right)\nabla\left(\frac{K_g}{\mu_g B_g}\right)\nabla P + B_w\frac{K_g}{\mu_g B_g}\nabla\left(\frac{1}{GWR}\right)\nabla P \qquad (14)$$

Where $\nabla(1/WGR)\nabla P$ can be neglected. Therefore Eq. (7) becomes

$$\nabla^2 P + \nabla \ln\left(\frac{K_g}{\mu_g B_g}\right)\nabla P = \frac{1}{3.6}\frac{C_t^* \phi}{\lambda_t}\frac{\partial P}{\partial t} \tag{15}$$

The gas saturation throughout the drainage area is increased steadily with time when the pressure front reached the boundary [16], therefore, the gas effective permeability can be assumed constant. For low pressure coal seams, the product of gas viscosity and Z-factor is also assumed to be constant [12], thus:

$$\frac{K_g}{\mu_g B_g} = \frac{K_g}{\mu_g Z}\frac{Z_{sc}T_{sc}}{P_{sc}T}P = \frac{K_g}{\mu_{g0}Z_0}\frac{Z_{sc}T_{sc}}{P_{sc}T}P = \alpha P \tag{16}$$

Where α is constant. Substituting Eq. (16) into (15) yields [12-14]

$$\nabla^2 P^2 = \frac{1}{3.6}\frac{C_t^* \phi}{\lambda_t}\frac{\partial P^2}{\partial t} \tag{17}$$

As seen in Eq. (17), the flow differential equation for middle and late stages is described by pressure squared, while in early stage, it is described by pressure only as seen in Eq. (13).

3.2 Approximation solution of pressure profiles

In order to solve the transient flow equations of 13 and 17, the concept of "continuous succession of steady states" [16, 17] is used. The pressure profile at any production time of CBM wells could be determined by pressure solution of steady-state flow until desorption area reaches the boundary. In the early stage of two-phase flow (including single phase water flow stage), the diffusivity equation is described by Eq. (13), therefore, the pressure solution for steady-state radial flow is given by the following:

$$P = P_{wf} + \frac{P_d - P_{wf}}{\ln\left(r_d/r_w\right)}\ln\left(r/r_w\right) \tag{18}$$

Where r_d is the radius of desorption area.

In the middle and late stages, the diffusivity equation is described by pressure squared approach (Eq. (17)); therefore, the pressure solution for steady-state radial flow is given by:

$$P^2 = P_{wf}^2 + \frac{P_d^2 - P_{wf}^2}{\ln\left(r_d/r_w\right)}\ln\left(r/r_w\right) \tag{19}$$

As we mentioned before, the equations (18) and (19) are for the pressure propagation in CBM wells in radial geometry with no hydraulic fracture stimulation. We have solved the same equations of 13 and 17 in elliptical geometry for the cases of fractured wells. It is reported that the pressure propagates in elliptical geometry when the well is vertical and hydraulically fractured [18-20]. For example, in the case of low permeability coal bed methane in Hancheng region in China, hydraulic fracturing is always necessary and commonly used to increase the production rate and make the development of CBM economical level. In order to transform the elliptical geometry into linear geometry we have used conformal transformation by the following equations [18-20]:

$$x = L \cdot ch\xi \cdot \cos\eta$$
$$y = L \cdot sh\xi \cdot \sin\eta \qquad (20)$$

The pressure profile in steady state flow in early stage and later stages are then given by:

$$\text{Early stage:}\quad P = P_{wf} + \frac{P_d - P_{wf}}{\xi_d - \xi_w}\left(\xi - \xi_w\right) \qquad (21)$$

$$\text{Middle and late stages:}\quad P^2 = P_{wf}^2 + \frac{P_d^2 - P_{wf}^2}{\xi_d - \xi_w}\left(\xi - \xi_w\right) \qquad (22)$$

Where ξ_w=0, the major and minor semi-axis of the elliptical desorption area are calculated by the following equations:

$$x_d = L \cdot ch\xi_d;\quad y_d = L \cdot sh\xi_d \qquad (23)$$

3.3 Desorption radius in vertical well with no fractures

For radial flow, the desorption front expands outward in circular geometry. If we consider the control volume, a fixed region in space (shaded area in Figure 2a), we may write

[The cumulative production] = [The volume of desorption gas] - [The volume of free gas remain in cleats]. The material balance formula in differential form is written as

$$dG_p = \left[\frac{P_d V_L}{P_L + P_d} - \frac{PV_L}{P_L + P} - \left(\phi S_g / B_g\right)\right] dV \qquad (24)$$

The volume of free gas remained in the cleats can be neglected because the cleat porosity is small (about 2% for Hancheng field) and the pressure of coal seam is low, thus, the Eq. (24) becomes:

$$dG_p = \left[\frac{P_d V_L}{P_L + P_d} - \frac{PV_L}{P_L + P} - \left(\phi S_g / B_g\right)\right] dV \approx \left(\frac{P_d V_L}{P_L + P_d} - \frac{PV_L}{P_L + P}\right) dV \qquad (25)$$

By integration of gas desorption in whole region, the cumulative production is given below:

$$G_p = 2\pi h \int_{r_w}^{r_d} \left(\frac{P_d V_L}{P_L + P_d} - \frac{PV_L}{P_L + P}\right) r dr \qquad (26)$$

Therefore, if all parameters are known, desorption radius (r_d) can be calculated by Eq. (26). For example, if the cumulative production G_p is obtained from field data, and pressure profiles are determined by Eq. (18) or (19), desorption radius r_d can be solved by iteration algorithm. Also, we need to mention that if r_d is calculated based on Eq. (18) (pressure approach), it will be the minimum value of desorption radius, while if r_d is calculated based on Eq. (19) (pressure squared approach), it will be the maximum value. Therefore, the minimum and maximum value of desorption radius can be estimated by combining Eq. (26) with Eq. (18) or Eq. (19) respectively.

3.4 Desorption area in vertical well with hydraulic fractures

For elliptical flow, the desorption front expands outward in elliptical form in the control volume, as shown in Figure 2b. If the free gas in cleat system is also neglected, the cumulative production in

whole desorption area is given by

$$G_p = \iint \left(\frac{P_d V_L}{P_L + P_d} - \frac{P V_L}{P_L + P} \right) dV \qquad (27)$$

Where $dV = h \cdot dA$， A represents the elliptical area as the following:

$$\left| \frac{\partial(x,\ y)}{\partial(\xi,\ \eta)} \right| = \begin{vmatrix} \frac{\partial x}{\partial \xi} & \frac{\partial x}{\partial \eta} \\ \frac{\partial y}{\partial \xi} & \frac{\partial y}{\partial \eta} \end{vmatrix} = \frac{L^2}{2} \left[ch(2\xi) - \cos(2\eta) \right]$$

Thus:

$$dV = h \cdot dA = h \frac{L^2}{2} \left[ch(2\xi) - \cos(2\eta) \right] d\xi d\eta \qquad (28)$$

Substituting Eq. (28) into Eq. (27)

$$G_p = \pi h L^2 \int_{\xi_w}^{\xi_d} \left(\frac{P_d V_L}{P_L + P_d} - \frac{P V_L}{P_L + P} \right) ch(2\xi) d\xi \qquad (29)$$

In Eq. (29), ξ_d is the unknown parameter. Then, the major semi-axis x_d and minor semi-axis y_d can be obtained from Eq. (23). Similar to radial case if ξ_d is calculated based on Eq. (21) (pressure approach), it is the minimum value of desorption radius, while if ξ_d is calculated based on Eq. (22) (pressure squared approach), it is the maximum value. Therefore， the minimum and maximum value of desorption area can be estimated by combining Eq. (29) with Eq. (21) or Eq. (22) respectively.

4. Numerical Simulation

Two CBM numerical models are built to show how the results from the developed analytical model are matched with a numerical simulation. The input data for two models are shown in Table 1. The first model (Model I) represents a CBM well located in a circular closed reservoir with uniform thickness and isothermal condition. In this simulation, the grids were radial and the drainage radius was set equal to 350m (Figure 3a). In the second model (Model Ⅱ), a hydraulic fractured well is considered with elliptical geometry as shown in Figure 3b. The fracture half-length is assumed to be 73.5 m. In this model, rectangular grids were used in a 700 m×700 m rectangular reservoir area.

Figure 4a shows the pressure profile after $4.8*10^5$ m^3 cumulative productions from model I. In this figure, the square dots represent the results from simulation, while the dashed line and solid line represent the results by our model for radial flow by pressure and pressure squared approaches respectively. In early times, the pressure approach was used until the 50^{th} day and the pressure squared approach was used for the later times. As it is seen, the results from the analytical model are good matched with numerical simulation. It is verified that the unsteady pressure profile during production can be approximated by the approaches of “pressure” or “pressure squared” in steady state condition.

Based on the cumulative production data, the desorption radius are calculated and compared to

the simulation results. As shown in Figure 4b, in early times when the gas production is not high, the pressure approach can match the simulation. However, in middle and late times, it is confirmed that the pressure squared approach is the proper methodology. In general, we can conclude that all simulation values are not less than the values from the pressure approach and also are not higher than the values from the pressure squared approach. Therefore, the pressure and pressure squared approaches can create a window for the maximum and minimum values of simulation.

For hydraulic fractured well of Model Ⅱ, as seen in Figure 5, it is confirmed that the major semi-axis of elliptical desorption area starts with fracture half-length (73.5m) and expands outward (Figure 5a), while the minor semi-axis starts from the wellbore radius (Figure 5b). It is also shown that the desorption area calculated by pressure squared approach is closer to the simulated results. The reason for this finding is that, since there is a large gas-water ratio in the early production stage as a result of hydraulic fracturing, the pressure approach is not applicable here.

5. Field Application

The development of coal-bed methane in China focuses mainly in two basins of Qinshui basin in Shanxi province and Ordos Basin in Northwest China. The Southeastern of Ordos Basin is Hancheng area where coal-bed methane reservoirs have been developed for several years. In this study, we have analyzed the data from four wells (A, B, C, and D) drilled in Hancheng area. The well locations are shown in Figure 6. Well A and B were put into production in August 18, 2005, while the production in well C and well were started in January 18, 2007, and in February 14, 2007 respectively.

As the first task in field data analysis, desorption area expansion of well A and B were analyzed before well C, and D were into production. The reservoir and well data including Langmuir constant P_L and V_L are shown in Table 1. Also, the desorption pressure is 1.4 MPa, the net thickness of well A and B are 5.40 m and 4.05 m respectively and the fracture half-length is assumed to be 60 m. To predict the desorption area, we have used our developed model based on the cumulative production and well bottom-hole pressure, and it is assumed that the desorption area of well A and well B are not interfered with each other. Figure 7 shows the major and minor semi-axis of desorption ellipse of well A and well B. It is seen that the difference between the major semi-axis and minor semi-axis decreases with time. After 250 days of production (January 18, 2007), the major semi-axis of desorption ellipse of well A ranges from 150.5 m to 188 m, while the minor semi-axis ranges from 138 m to 178 m. Similarly, the major semi-axis of well B ranges from 170 m to 215 m, while the minor semi-axis ranges from 159 m to 206.5 m. Figure 8a and 8b illustrated the maximum and minimum of desorption area in January 18, 2007 respectively. In this case, the desorption fronts in well A and B have been interfered with each other in the 390th day. Also, the desorption front of well A has reached the desorption area of well D. Also the desorption front in direction of fracture orientation of well C interferes with well A right after the production due to the effect of hydraulic fracturing. In the latter case, the distance between desorption front of well A and well B is only 13.0 m apart, therefore, the two wells will interfere with each other soon. Furthermore, the distance between desorption front of

well A and fracture tip of well C is 29.5 m while the distance between desorption front of well A and the location of well D is 32.0 m. In general, the proposed models can be used as a simple and fast technique to predict the desorption area expansion.

6. Conclusions

1) An analytical model is developed for the prediction of desorption area in CBM reservoirs. The model is based on simplified approach of two-phase flow equations when desorption is controlling the gas production. Our model is developed for both non stimulated and hydraulically fractured vertical wells.

2) Unlike the numerical simulation, the developed model is based on material balance and does not require cleat permeability and gas-water relative permeability curves. The model is validated by a good match with numerical simulation. It was found that in early production, the pressure approach can match the simulation; however, in middle and late times, the pressure squared approach matches the simulation.

3) The proposed model was applied on a CBM well group in Hancheng field, China. It is found that desorption area expands with elliptical geometry. The size of desorption area has been estimated by the gas production and bottom-hole pressure data. The results predict that well A and well B have interfered with each other after 525 days of production. Also, it is predicted that Well C and well D will be in contact with the desorption area of well A if they are put into the production.

4) It is also concluded that although if the desorption front reaches the boundary (drainage area interference), the proposed models are not applicable, the desorption area and the timing before the start of interference can be determined.

Acknowledgements

This paper was sponsored by Special Grand National Science Technology Project (2011ZX05038-004) and the national basic research program of China (2009CB219606). We acknowledge the support of China University of Petroleum (Beijing) for the permission to publish this paper.

Nomenclature

A the area of desorption area, m^2
b Langmuir isotherm constant, MPa^{-1}
B_g gas FVF, fraction
B_w water FVF, fraction
C_d desorption compressibility, MPa^{-1}
C_t* modified total compressibility, MPa^{-1}
C_f rock compressibility, MPa^{-1}
C_g gas compressibility, MPa^{-1}
C_w water compressibility, MPa^{-1}
G_p cumulative production, m^3
K absolute permeability, md

K_{rg} effective permeability to gas, dimensionless
K_{rw} effective permeability to water, dimensionless
L fracture half-length, m
P reservoir pressure, MPa
P_{sc} reservoir pressure at standard conditions, MPa
P_d critical desorption pressure, MPa
P_{wf} well bottom hole pressure, MPa
P_L Langmuir pressure, MPa
q_d quantity of desorption gas from matrix to cleat, $m^3/(m^3 \cdot h)$
r radius, m
r_d desorption radius, m
r_w wellbore radius, m
S_g gas saturation, fraction
S_w water saturation, fraction
T_{sc} absolute temperature, K
T absolute temperature at standard conditions, K
t production time, days
V the volume of desorption area, m^3
V_m Langmuir pressure, m^3/m^3
x, y Cartesian coordinate, m
Z compressibility factor, fraction
Z_{sc} compressibility factor at standard conditions, fraction

Greek symbols

μ_g gas viscosity, mPa·s
μ_w water viscosity, mPa·s
φ cleat porosity, fraction
ξ、η elliptical coordinates, m
λ_t total mobility of gas and water, md/(mpa·s)

References

[1] Joseph C. Behavior of coal-gas reservoirs. In: SPE 1973, presented at the SPE Eastern Regional Meeting, Pittsburgh, Pennsylvania; November 2-3, 1967.

[2] Karn FS, Friedel RA, Thames BM, Sharkey AG. Gas transport through sections of solid coal. Fuel 1970; 49(3):249-256.

[3] McKee, C.R., Bumb, A.C. Flow-Testing Coalbed Methane Production Wells in the Presence of Water. SPE Formation Evaluation 1987; 2(4): 599-608.

[4] Gas Research Institute. A guide to coalbed methane reservoir engineering. GRI reference No.GRI-94/0397, Chicago, Illinois ; 1994.

[5] Seidle JP. Long-term gas deliverability of a dewatered coalbed. Journal of Petroleum Technology 1993; 45(6): 564-569.

[6] Spivey JP, Semmelbeck ME. Forecasting long-term gas production of dewatered coal seams and fractured gas shales. In: SPE 29580, presented at the Low Permeability Reservoirs Symposium, Denver, Colorado; March 19-22, 1995.

[7] Luo Z, Yang X, Zhao J, et al. Research on numerical simulation of coalbed methane well. Journal of China University of Mining & Technology 2000; 29(3):306- 309.

[8] Gentzis T, Bolen D. The use of numerical simulation in predicting coalbed methane producibility from the Gates coals, Alberta Inner Foothills, Canada: Comparison with Mannville coal CBM production in the Alberta Syncline. International Journal of Coal Geology 2008; 74:215-236.

[9] Zuber MD. Production characteristics and reservoir analysis of coalbed methane reservoirs. International Journal of Coal Geology 1998; 38: 27-45.

[10] Ziarani AS, Aguilera R, Clarkson, CR. Investigating the effect of sorption time on coalbed methane recovery through numerical simulation. Fuel 2011; 90:2428-2444.

[11] Clarkson CR, Rahmanian M, Kantzas A, Morad K. Relative permeability of CBM reservoirs: Controls on curve shape. International Journal of Coal Geology 2011; 88: 204-217.

[12] Al-Khalifa AJ, Home RN, Aziz K. Multiphase well test analysis: pressure and pressure-squared methods. In: SPE 18803, Presented at the SPE California Regional Meeting, Bakersfield, California; April 6-7, 1989.

[13] Sun Z, Jia C, Li X, et al. Unconventional Oil & Gas Exploration and Development. Beijing: Petroleum Industry Press; 2011.

[14] Hu X, Zhen S, Hu S, et al. Application of Quadratic Pressure Method in Well Test Interpretation of Gas-water Two-phase Flow in Coal Seam. Journal of Oil and Gas Technology 2011; 33(2):118-122.

[15] Seidle JP. A numerical study of coal-bed dewatering. In: SPE 24358, presented at the SPE Rocky Mountain Regional Meeting, Casper, Wyoming; 18-21 May, 1992.

[16] Muskat, M. The flow of homogeneous fluids through porous media. New York: McGraw-Hill Book Co. Inc.; 1937.

[17] Ge J. Fluid flow in porous media. Beijing: Petroleum Industry Press; 1982.

[18] Kucuk F, Brigham WE. Transient Flow in Elliptical Systems. SPE Journal 1979; 19(6):401-410.

[19] Liao Y, Lee WJ. Depth of investigation for elliptical flow problems and its applications to hydraulically fractured wells. In: SPE 27908, presented at the SPE Western Regional Meeting, California, USA; March 23-25, 1994.

[20] Song F, Liu C, Wu B. The elliptic transient flow of vertically fractured well in anisotropic reservoir. Petroleum Exploration and Development 2001; 28(1):57-59.

Table 1- input data for numerical simulation

Parameter	Model Ⅰ	Model Ⅱ
Langmuir volume, V_L(m^3/m^3)	33	33
Langmuir Pressure, P_L (MPa)	2.4	2.4
Formation thickness, h(m)	8	8
Desorption pressure, P_d (MPa)	4	1.5
Initial pressure, P_i (MPa)	4.5	3
Well radius, r_w (m)	0.085	0.085
Flowing bottom-hole pressure , P_{wf} (MPa)	0.3	0.3

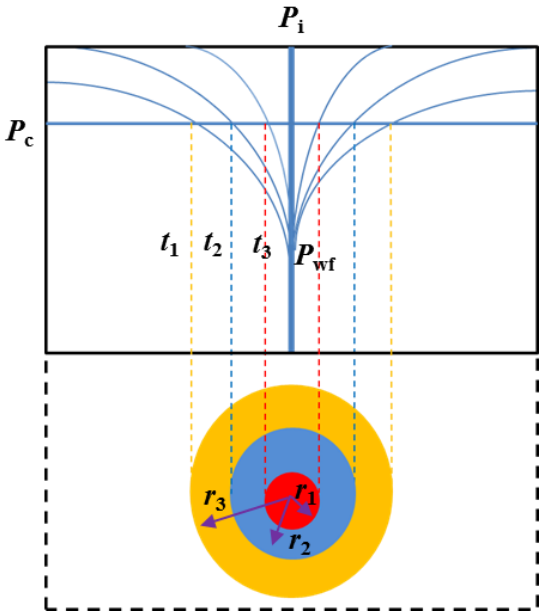

Fig.1. The schematic of desorption area expansion in a CBM well

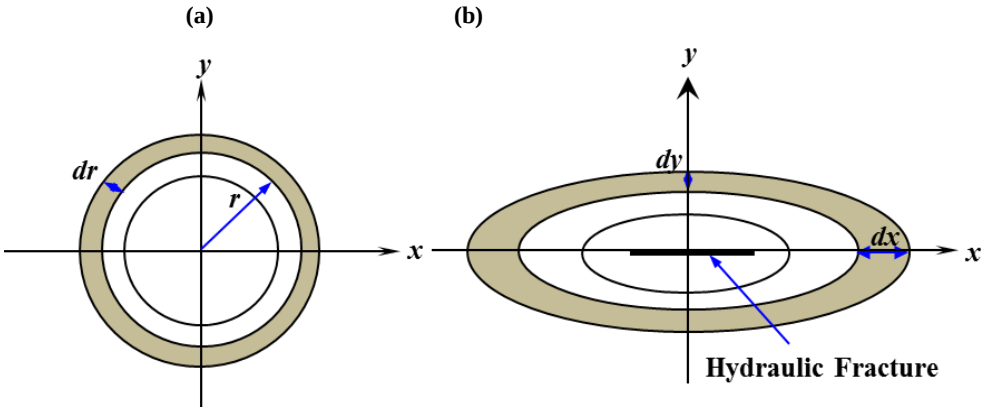

Fig.2. The infinitesimal element of gas flow in a CBM reservoir around a wellbore, (A) Radial; (B) Elliptical.

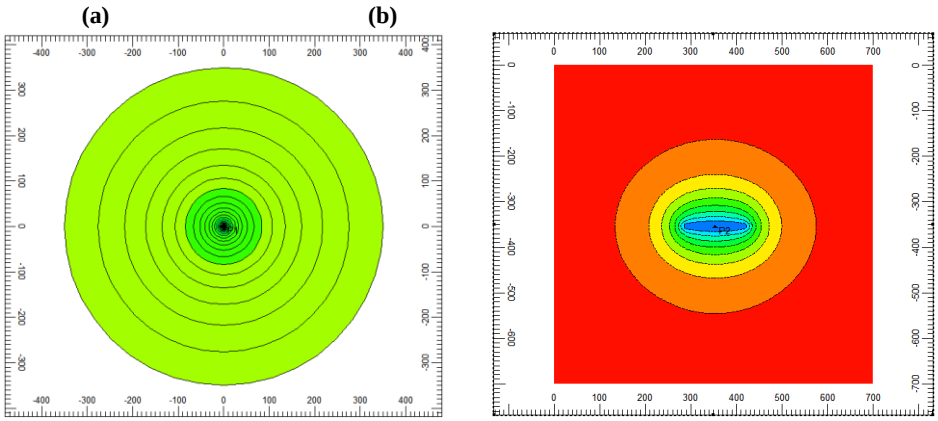

Fig.3. Well model geometry: (A) radial geometry, (B) elliptical geometry

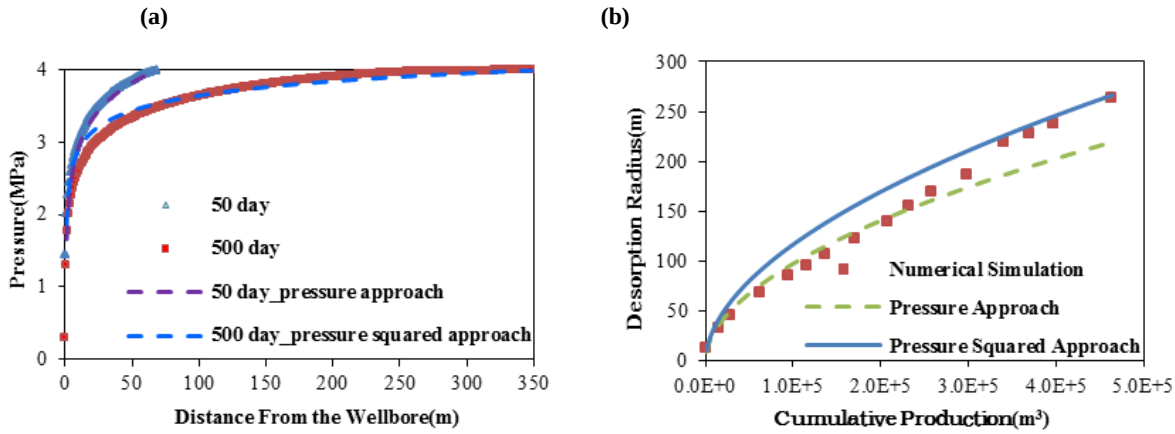

Fig.4. The comparison of the results with numerical simulation: (a) Pressure profile in desorption area; (b) Relationship between desorption radius and cumulative production

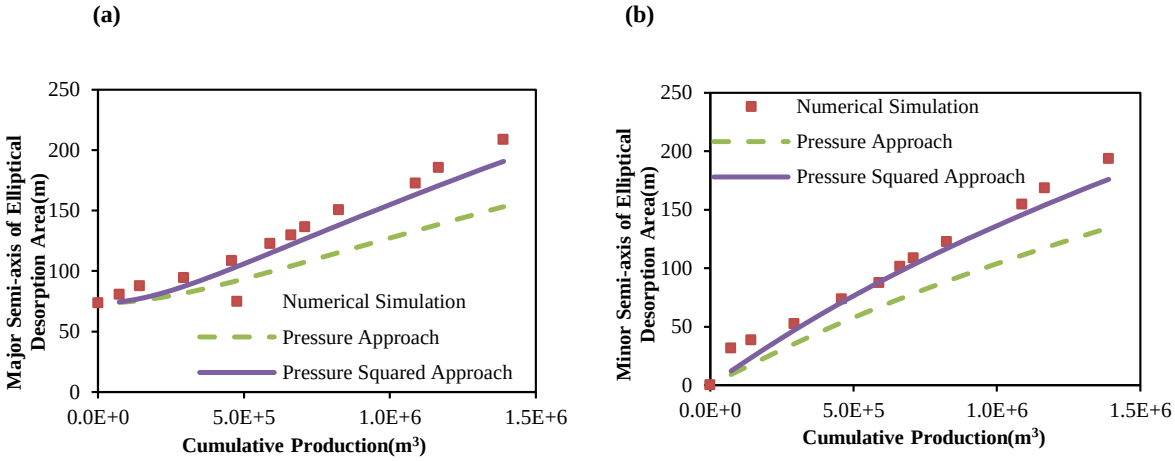

Fig.5. The comparison of the results with numerical simulation: (a) Major semi-axis of elliptical desorption area; (b) Minor semi-axis of elliptical desorption area

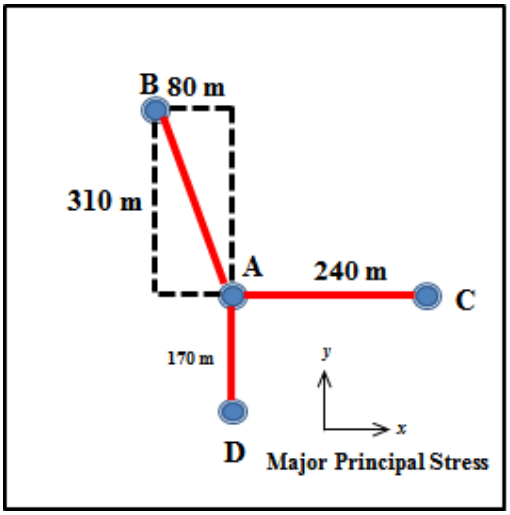

Fig.6. The schematic of different well locations

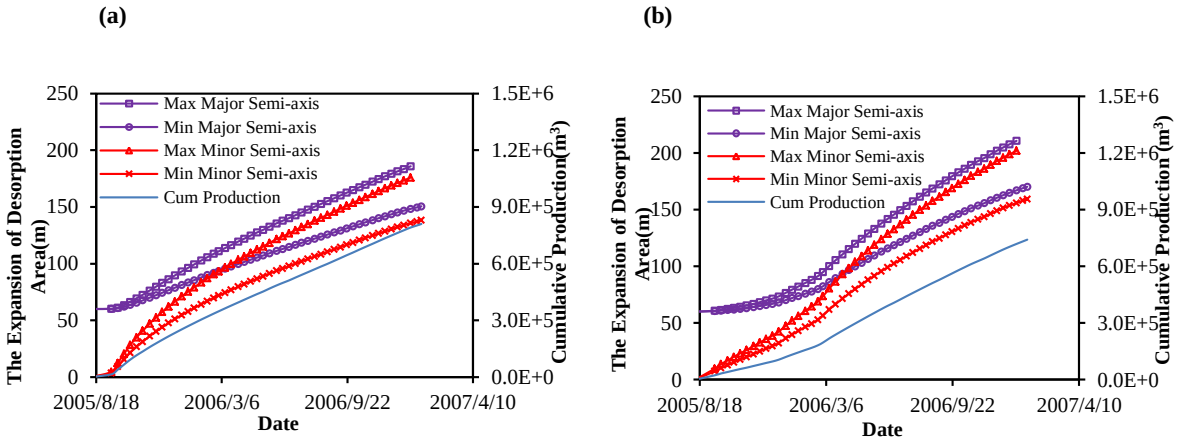

Fig.7. The expansion of desorption area with time: (a) Well A; (b) Well B

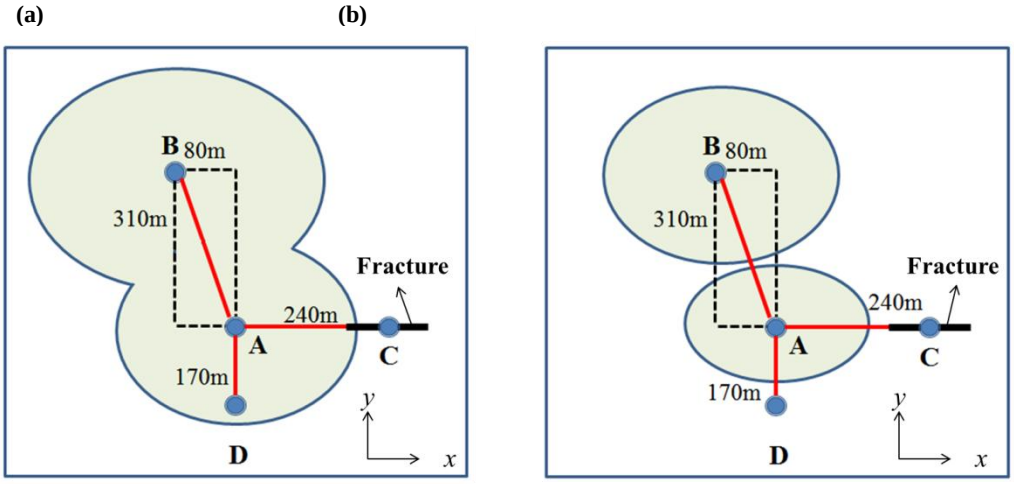

Fig.8. The prediction of desorption area after 525 days: (a) Maximum; (b) Minimum